HOT-REFRESH MODEL UPGRADES WITH REGRESSION-FREE COMPATIBLE TRAINING IN IMAGE RETRIEVAL

Anonymous authors
Paper under double-blind review

ABSTRACT

The task of hot-refresh model upgrades of image retrieval systems plays an essential role in the industry but has never been investigated in academia before. Conventional cold-refresh model upgrades can only deploy new models after the gallery is overall backfilled, taking weeks or even months for massive data. In contrast, hot-refresh model upgrades deploy the new model immediately and then gradually improve the retrieval accuracy by backfilling the gallery on-the-fly. Compatible training has made it possible, however, the problem of model regression* with negative flips poses a great challenge to the stable improvement of user experience. We argue that it is mainly due to the fact that new-to-old positive query-gallery pairs may show less similarity than new-to-new negative pairs. To solve the problem, we introduce a Regression-Free Compatible Training (RFCT) method to properly constrain the feature compatibility while reducing negative flips. The core is to encourage the new-to-old positive pairs to be more similar than both the new-to-old negative pairs and the new-to-new negative pairs. An efficient uncertainty-based backfilling strategy is further introduced to fasten accuracy improvements. Extensive experiments on large-scale retrieval benchmarks (*e.g.*, Google Landmark) demonstrate that our RFCT effectively alleviates the model regression for one more step towards seamless model upgrades.

1 INTRODUCTION

With the rapid development of deep learning, image retrieval algorithms have shown great success in large-scale industrial applications, *e.g.*, face recognition (Sun et al., 2014a;b), object re-identification (Li et al., 2014; Zheng et al., 2015), image localization (Arandjelovic et al., 2016). Model upgrades are essential to improve user experience in those applications. By properly leveraging massive training data and improved network architectures, the retrieval performances could be well boosted.

Generally, once the model updates, the process of "backfilling" or "re-indexing" is called for offline re-encoding the gallery image features with the new model. The retrieval system can only benefit from the new model after the gallery is overall backfilled, which may cost weeks or even months for billions of industry images in practice. The above process is termed *cold-refresh* model upgrades.

To harvest the reward of the new model immediately, Shen et al. (2020) introduces the compatible representation learning to train the new model with backward compatibility constraints, so that queries encoded by the new model can be directly indexed by the old gallery features. Meanwhile, as the new features and old features are interchangeable with each other, the gallery images can be backfilled on-the-fly, and the retrieval performances would be gradually improved to approach the optimal accuracy of the new model, dubbed as *hot-refresh* model upgrades (see Figure 1 (a)).

Although existing compatible training methods (Meng et al., 2021; Shen et al., 2020) make it possible to upgrade the model in a hot-refresh manner, they still face the challenge of *model regression* (Yan et al., 2020; Li & Hoiem, 2018), which is actually caused by *negative flips*, *i.e.*, queries correctly indexed by the old model are incorrectly recognized by the new model (see Figure 1 (b)).

*Throughout this paper, the term *model regression* indicates the degradation of retrieval performance when the hot-refresh model upgrades proceed.

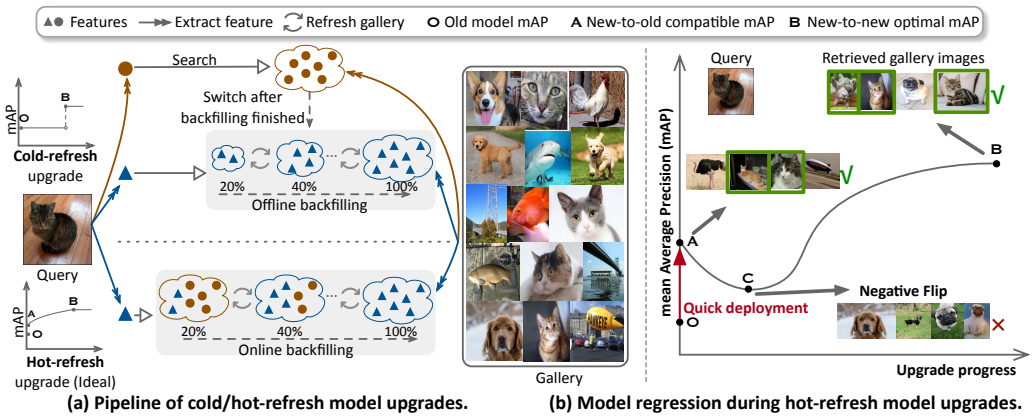

Figure 1: **(a)** The illustration of cold-refresh and hot-refresh model upgrades. **(b)** The problem of model regression with negative flips in hot-refresh model upgrading procedure of image retrieval systems, where queries retrieved correctly by the old model fail during the upgrade process.

We claimed that, during the procedure of hot-refresh model upgrades, the negative flips occur when the new-to-new similarities between negative query-gallery pairs are larger than the new-to-old similarities between compatible positive query-gallery pairs. To solve the problem, we introduce a **R**egression-**F**ree **C**ompatible **T**raining (**RFCT**) method to effectively reduce the negative flips for compatible representation learning and further improve the hot-refresh model upgrades with faster and smoother accuracy convergence in image retrieval systems.

Specifically, the conventional backward-compatible regularization is generally designed to pull the new-to-old positive pairs closer and push the new-to-old negative pairs apart from each other. To reduce negative flips during the online gallery backfilling, we improve the backward-compatible regularization by enforcing the new-to-old positive pairs to be more similar than both the new-to-old negative pairs and the new-to-new negative pairs. To further improve the user experience during the model upgrades, we introduce an uncertainty-based hot-refresh backfilling strategy, which re-indexes the gallery images following "the-poor-first" policy. To measure the refresh priority of gallery images in a lightweight manner, we feed the old gallery features into the new classifier (one fully-connected layer in general), yielding the probability distribution on new classes. Even though ground-truth classes may not exist for the old gallery features, we can assume that more discriminative old features are expected to have sharper probability vectors given their compatible latent space. Uncertainty estimation (*e.g.*, Entropy-based) is utilized here to evaluate the sharpness of the probability vectors, and gallery images with larger uncertainty should have higher priority for backfilling. Experimental results on large-scale image retrieval benchmarks (*i.e.*, Google Landmark v2 (Weyand et al., 2020), Paris6k, and Oxford5k (Philbin et al., 2008; 2007)) demonstrate the effectiveness of our RFCT method in alleviating the problem of model regression for hot-refresh model upgrades.

Our contributions can be summarized three-fold. (1) We study the model regression problem in hot-refresh model upgrades of image retrieval systems for the first time. (2) A regression-free backward-compatible regularization is proposed to alleviate the issue of negative flips during compatible training. (3) An uncertainty-based backfilling strategy is introduced to further improve the user experience with "the-poor-first" hot refresh.

2 Related Works

Compatible Representation Learning. The task of compatible representation learning aims at encoding new features that are interoperable with the old features. It breaks the inherent cold-refresh way of model iteration in the industry - the benefit of new models can be immediately reaped in a backfill-free manner. Shen et al. (2020) first formulated the problem of backward-compatible learning and proposed to utilize the old classifier for supervising the compatible feature learning. Budnik & Avrithis (2020) made an effort to reduce the gap between the large model and a small one without the parametric classifier. Wang et al. (2020) introduced a projection head to transform the old

features to be compatible with the new ones. Li et al. (2020b) proposed a framework, namely "Feature Lenses", to encourage image representations transformation-invariant. To balance the trade-off between performance and efficiency, Duggal et al. (2021) designed a compatibility-aware neural architecture search scheme to improve the compatibility of models with different sizes. However, since existing compatible algorithms for image retrieval have not investigated the application of hot-refresh model upgrades, the problem of model regression has been overlooked.

Model Regression. Model upgrades play a vital role in improving the performance of industrial applications, where the issue of model regression inevitably harms the user experience. Yan et al. (2020) studied the problem of model regression in image classification, where the negative flips indicate the images correctly classified by the old model but misclassified by the new model. A method, namely focal distillation, was introduced to encourage model congruence on positive samples. Srivastava et al. (2020) also investigated the model regression in classification and proposed a new metric to evaluate the regression effects. Xie et al. (2021) probed the model regression problem in natural language processing. The works mentioned above all focused on the classification tasks. Directly employing their methods on the retrieval tasks leads to sub-optimal performances. Moreover, they did not need to consider hot-refresh gallery backfilling in image classification.

Active Learning. Our uncertainty-based backfilling strategy is related to active learning. As the real world is teeming with unlabeled data, active learning makes efforts to achieve better performance with fewer annotated samples by choosing valuable samples actively (Settles, 2009). Active learning has been widely adopted in deep learning tasks, *e.g.*, object detection (Holub et al., 2008), text classification (Zhu et al., 2008), and image classification (Cao et al., 2020). Though obtaining the priority of samples is a common issue between active learning and gallery backfilling, the latter focuses more on enjoying benefits in model upgrades with minimal computational overhead.

Image Retrieval. The task of image retrieval requires searching images of the same content or object from a large-scale database based on their feature similarities, given images of interest. It is a fundamental task for many visual applications, *e.g.*, face recognition (Guillaumin et al., 2009; Cui et al., 2013), person re-identification (Bak & Carr, 2017; Liu et al., 2017), image localization (Arandjelovic et al., 2016; Ge et al., 2020b). Deep learning-based methods improve the accuracy of image retrieval by casting it as metric learning tasks (Gordo et al., 2016; Chen et al., 2018; Brown et al., 2020), architecture design/search tasks (Zhou et al., 2019), or self-/semi-supervised learning tasks (Ge et al., 2020c;a). Although many efforts have been made to improve retrieval performance, few people pay attention to the bottleneck of model upgrades in industrial applications.

3 Hot-Refresh Model Upgrades of Image Retrieval Systems

Given images of interest (referred to as query $\mathcal{Q}$), image retrieval targets correctly recognizing images of the same content or objects from a large-scale database (referred to as gallery $\mathcal{G}$). An image encoder $\phi(\cdot)$ is employed to map the images into feature vectors. Then, the dot product of normalized vectors is used for measuring the similarity between query and gallery images for ranking.

3.1 Hot-Refresh Model Upgrades with Compatible Representations

Let ϕ_{old} to be the old image encoder that was deployed in the retrieval system and ϕ_{new} to be a stronger new encoder which is expected to replace the old one. We denote the evaluation metric for image retrieval, *e.g.*, mean Average Precision (mAP), as $\mathcal{M}(\cdot,\cdot)$. The accuracy of the old system is denoted as $\mathcal{M}(\mathcal{Q}_{\text{old}}, \mathcal{G}_{\text{old}})$, where $\mathcal{Q}_{\text{old}}, \mathcal{G}_{\text{old}}$ are the sets of query and gallery features embedded by ϕ_{old}, respectively. The new encoder shows an improved accuracy of $\mathcal{M}(\mathcal{Q}_{\text{new}}, \mathcal{G}_{\text{new}})$. In conventional **cold-refresh** model updating pipeline, offline backfilling the gallery images from $\mathcal{G}_{\text{old}}$ to $\mathcal{G}_{\text{new}}$ may take months for the massive data in industry applications, reducing the efficiency of the retrieval system upgrades to a large extent.

Thanks to the compatible representation learning (Shen et al., 2020), query features encoded by the new encoder (*i.e.*, $\mathcal{Q}_{\text{new}}$) can be directly compared to the old gallery features (*i.e.*, $\mathcal{G}_{\text{old}}$). The retrieval system can benefit from the new encoder immediately in a backfill-free manner, significantly

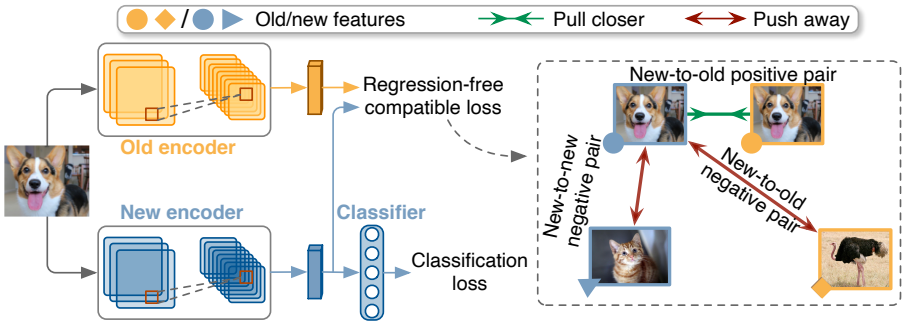

Figure 2: The illustration of our Regression-Free Compatible Training (RFCT) framework.

accelerating the model iteration at the expense of the optimal performance,

$$\mathcal{M}(\mathcal{Q}_{\text{old}}, \mathcal{G}_{\text{old}}) < \mathcal{M}(\mathcal{Q}_{\text{new}}, \mathcal{G}_{\text{old}}) < \mathcal{M}(\mathcal{Q}_{\text{new}}, \mathcal{G}_{\text{new}}). \tag{1}$$

Given that the new features and old features are interchangeable due to their compatibility, the gallery images can be backfilled on-the-fly to progressively improve the retrieval accuracy to achieve the optimal performance of the new model,

$$\begin{aligned}\mathcal{M}(\mathcal{Q}_{\text{new}}, \mathcal{G}_{\text{old}}) \rightarrow \cdots \rightarrow \mathcal{M}(\mathcal{Q}_{\text{new}}, \mathcal{G}_{\text{new}}^{20\%} \cup \mathcal{G}_{\text{old}}^{80\%}) \rightarrow \cdots \rightarrow \mathcal{M}(\mathcal{Q}_{\text{new}}, \mathcal{G}_{\text{new}}^{50\%} \cup \mathcal{G}_{\text{old}}^{50\%}) \rightarrow \\ \cdots \rightarrow \mathcal{M}(\mathcal{Q}_{\text{new}}, \mathcal{G}_{\text{new}}^{80\%} \cup \mathcal{G}_{\text{old}}^{20\%}) \rightarrow \cdots \rightarrow \mathcal{M}(\mathcal{Q}_{\text{new}}, \mathcal{G}_{\text{new}}).\end{aligned} \tag{2}$$

The above process is termed as **hot-refresh** model upgrades, where $\mathcal{G}_{\text{new}}^{20\%}$ indicates the 20% of images in the gallery have been re-indexed by the new model ϕ_{new}.

3.2 Model Regression with Negative Flips

Ideally, the performance of the retrieval system should be smoothly upgraded along with the gallery online backfilling, and the user experience would be continuously improved. However, we observe the phenomenon of **model regression** especially in the early backfilling stages, that is, the accuracy degrades when part of the gallery images are refreshed, *e.g.*,

$$\mathcal{M}(\mathcal{Q}_{\text{new}}, \mathcal{G}_{\text{new}}^{20\%} \cup \mathcal{G}_{\text{old}}^{80\%}) < \mathcal{M}(\mathcal{Q}_{\text{new}}, \mathcal{G}_{\text{old}}). \tag{3}$$

It is actually due to the **negative flips**, where some query images correctly retrieved by the old model are incorrectly indexed by the new model during the upgrade process. We figure out the reason for the negative flips: new-to-old query-gallery positive pairs are less similar than new-to-new query-gallery negative pairs, *i.e.*, there exists a query x_q that satisfies

$$\langle \phi_{\text{new}}(x_q), \phi_{\text{old}}(x_g^{\text{pos}}) \rangle < \langle \phi_{\text{new}}(x_q), \phi_{\text{new}}(x_g^{\text{neg}}) \rangle, \tag{4}$$

where x_g^{pos} is the positive gallery sample, x_g^{neg} is the negative gallery sample, and $\langle \cdot, \cdot \rangle$ denotes the cosine similarity of two normalized feature vectors. In the case of Eq. (3), $\phi_{\text{new}}(x_q) \in \mathcal{Q}_{\text{new}}$, $\phi_{\text{old}}(x_g^{\text{pos}}) \in \mathcal{G}_{\text{old}}^{80\%}$ and $\phi_{\text{new}}(x_g^{\text{neg}}) \in \mathcal{G}_{\text{new}}^{20\%}$.

4 Methodology

We introduce a regression-free compatible training approach (Figure 2) for tackling the challenge of model regression in the hot-refresh model upgrades of image retrieval systems, which has essential impacts on the user experience but was ignored by previous compatible training methods. Our key idea is to encourage the new-to-old positive pairs to be more similar than not only the new-to-old negative pairs but also the new-to-new negative pairs. In addition, an uncertainty-based strategy is proposed to backfill the gallery in "the-poor-first" manner, in order to fasten accuracy improvements.

4.1 Revisit Conventional Compatible Training

Being cast as either the metric learning task (Budnik & Avrithis, 2020) or the transformation learning task (Wang et al., 2020), the core of existing compatible training methods is to encourage the

new feature of an image to approach the old features of the intra-class images while keeping away from the old features of different classes. Without the loss of retrieval accuracy, we treat the compatible training as an instance discrimination task in large-scale retrieval tasks in order to improve the training efficiency, *i.e.*, the positive pair is the new and old features of the same instance as it is hard to make sure intra-class instances exist in the same mini-batch without a pre-sampler. The negative pair is built by the new and old features of inter-class instances in the mini-batch. We denote $\mathcal{T}$ as the training set and $\mathcal{B}$ as the mini-batch. Given an anchor image $x \in \mathcal{T}$, we can formulate the backward-compatible regularization as a contrastive loss,

$$\mathcal{L}_{\text{comp}}(x) = -\log \frac{\exp(\langle \phi_{\text{new}}(x), \phi_{\text{old}}(x) \rangle / \tau)}{\exp(\langle \phi_{\text{new}}(x), \phi_{\text{old}}(x) \rangle / \tau) + \sum_{k \in \mathcal{B} \setminus x} \exp(\langle \phi_{\text{new}}(x), \phi_{\text{old}}(k) \rangle / \tau)}, \tag{5}$$

where τ is a temperature hyper-parameter. With the above regularization, ϕ_{new} is trained to embed new features on the same latent space as the old features. However, they ignore the relation between new-old and new-new similarities, facing the risk of negative flips during model upgrading.

4.2 Regression-Free Compatible Training

Regression-Free Compatibility Regularization. To constrain the feature compatibility and reduce negative flips at the same time, we improve the conventional backward-compatible loss by adding new-to-new negative pairs as an extra regularization term. Such an improved backward-compatible loss provides regression-free regularization during training, which is formulated as

$$\mathcal{L}_{\text{rf-comp}}(x) = \tag{6}$$
$$-\log \frac{\exp(\langle \phi_{\text{new}}(x), \phi_{\text{old}}(x) \rangle / \tau)}{\exp(\langle \phi_{\text{new}}(x), \phi_{\text{old}}(x) \rangle / \tau) + \sum_{k \in \mathcal{B} \setminus x} \Big(\exp(\langle \phi_{\text{new}}(x), \phi_{\text{old}}(k) \rangle / \tau) + \exp(\langle \phi_{\text{new}}(x), \phi_{\text{new}}(k) \rangle / \tau) \Big)}.$$

In such a way, the new and old compatible positive pairs are trained to achieve more prominent similarities than both new-to-old and new-to-new negative pairs. The issue of negative flips can be alleviated properly when the gallery backfilling proceeds, *i.e.*, the gallery is a mix-up of both old and new features. We do not specifically constrain the new-to-new positive pairs to be closer than new-to-old negative pairs, as the new features are generally trained to be more discriminative than the old ones in order to achieve the model upgrading purpose. Thus, the new-to-new positives are naturally to achieve larger similarities than new-to-old negatives.

Overall Training Objective. Besides the compatibility constraints, we also need the ordinary training regularization for image retrieval tasks to maintain the distinctiveness of the new feature representations. Following the strong benchmark in (Weyand et al., 2020), we choose the classification as a pretext task during training. Specifically, we adopt a fully-connected layer as the classifier, denoted as $\omega_{\text{new}} : \mathbf{f} \rightarrow \{1, \cdots, C\}$, where C is the number of classes of the new training dataset. The classification loss for the pretext task is formulated as

$$\mathcal{L}_{\text{cls}}(x) = \ell_{\text{ce}}\Big(\omega_{\text{new}} \circ \phi_{\text{new}}(x), y(x)\Big), \tag{7}$$

where ℓ_{ce} denotes the cross-entropy loss and $y(x)$ is the ground-truth label for x. The overall training objective function for our regression-free compatible training framework is,

$$\mathcal{L}(x) = \mathcal{L}_{\text{cls}}(x) + \lambda \mathcal{L}_{\text{rf-comp}}(x), \tag{8}$$

where λ is the loss weight. New models trained towards the above objectives enable better hot-refresh upgrades of image retrieval systems by properly alleviating the problem of model regression.

4.3 Uncertainty-based Backfilling

In order to further fasten the accuracy convergence during the hot-refresh model upgrades, we propose to refresh the gallery following "the-poor-first" priority, *i.e.*, images with non-discriminative features are expected to be re-encoded first. Given the massive data in industrial applications, we need to quickly measure the distinctiveness of old gallery features in a relatively lightweight way. An uncertainty-based strategy is therefore introduced to measure the priority for backfilling the gallery.

We claim that the confidence of class probabilities represents the feature distinctiveness to some extent. Since the old and new latent spaces are directly comparable after compatible training, we can produce the class probabilities of the old gallery features by feeding them into the trained new classifier ω_{new}. Although the ground-truth classes of the gallery images are generally non-overlapped with the new training dataset and even unknown, we can assume that more discriminative features should have sharper class probability vectors. Inspired by the "uncertainty sampling" (Settles, 2009), we evaluate the sharpness of the probability vectors using the uncertainty estimation metrics. Samples with larger uncertainty scores will be assigned higher priority to be backfilled. We consider three common ways of measuring uncertainty in this paper.

Least Confidence Uncertainty. It considers the gap between 100% and the probability of the predicted class as the uncertainty score for each sample, formulated as

$$\mathcal{U}_{lc}(f_g) = 1 - \text{softmax}[\omega_{\text{new}}(f_g)]^1, \quad f_g \in \mathcal{G}_{\text{old}}, \tag{9}$$

where $\text{softmax}[\cdot]^k$ denotes the probability of rank k-th confident class.

Margin of Confidence Uncertainty. It measures the uncertainty of class probabilities by the difference between the top-2 confident predictions,

$$\mathcal{U}_{mc}(f_g) = 1 - (\text{softmax}[\omega_{\text{new}}(f_g)]^1 - \text{softmax}[\omega_{\text{new}}(f_g)]^2), \quad f_g \in \mathcal{G}_{\text{old}}, \tag{10}$$

Entropy-based Uncertainty. The above metrics only consider the top-1 or top-2 classes, while the Entropy-based uncertainty measurement takes the overall probability distribution into consideration.

$$\mathcal{U}_{e}(f_g) = -\sum_{i}^{C} \text{softmax}[\omega_{\text{new}}(f_g)]^i \cdot \log(\text{softmax}[\omega_{\text{new}}(f_g)]^i), \quad f_g \in \mathcal{G}_{\text{old}}, \tag{11}$$

where C is the number of classes in new training set.

5 EXPERIMENTS

5.1 IMPLEMENTATION DETAILS

Training Data. Google Landmark v2 (Weyand et al., 2020), GLDv2 in short, is a large-scale public dataset for landmark retrieval. Following the setup in (Jeon, 2020), we use a clean subset of GLDv2, dubbed GLDv2-clean, which consists of 1,580,470 samples with 81,313 classes. In this paper, we investigate three different kinds of data allocations for training the old model and the new model, covering most scenarios of model upgrades in practice. (1) **Expansion**: the new training set is an expansion of the old training set. We randomly sample 30% of images as the old training set, and use the 100% of images as the new training set. (2) **Open-data**: the new training data are excluded from the old training data, but they share the same classes. We randomly sample 30% of each class as the old training set, and use the rest 70% of each class as the new training set. (3) **Open-class**: the new training data and classes are both excluded from the old ones. We randomly sample 30% of classes for the old model training, and images of the rest 70% of classes are utilized for the new model training. The training data details can be found in Table 1.

Allocation type	Old train-set		New train-set	
	# images	# classes	# images	# classes
Expansion	445,419	81,313	1,580,470	81,313
Open-data	445,419	81,313	1,135,051	81,313
Open-class	472,604	24,393	1,107,866	56,920

Table 1: Three different allocations for the training data, where all the images are sampled from GLDv2-clean. The "expansion" and "open-data" setups share the same old training set.

Testing Data. We evaluate the trained models on three test sets, including GLDv2-test, Oxford5k, and Paris6k. GLDv2-test contains 761,757 gallery images and 750 query images. Following the test protocol in (Radenović et al., 2018), we use the medium testing with 70 queries for both Oxford5k and Paris6k. Oxford5k (Philbin et al., 2007) contains 5,007 gallery images, and Paris6k (Philbin et al., 2008) consists of 6,357 gallery images.

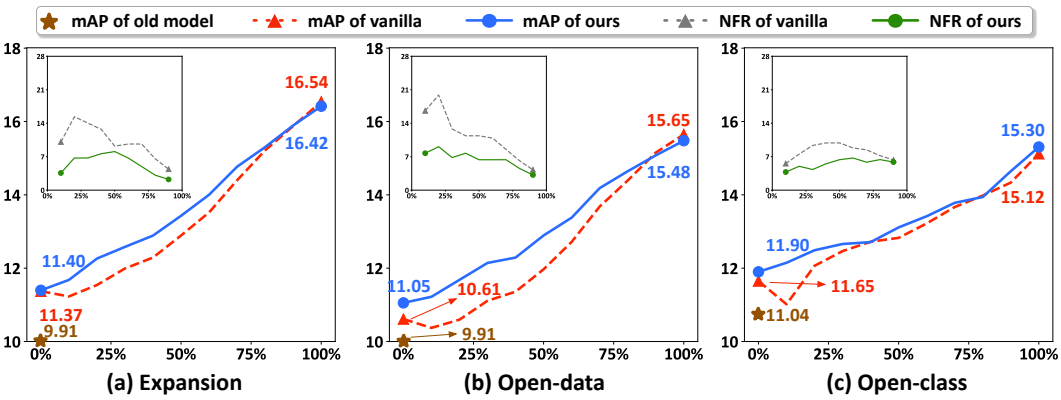

Figure 3: The trend of retrieval performance during the hot-refresh model upgrades (R50-R101) on GLDv2-test, in terms of mAP(↑) and NFR(↓). It can be observed that the models trained with vanilla compatibility regularization (*i.e.*, "vanilla") suffer from the model regression significantly. In contrast, the models trained with our regression-free compatibility regularization (*i.e.*, "ours") mitigate the model regression to some extent by properly reducing the negative flips.

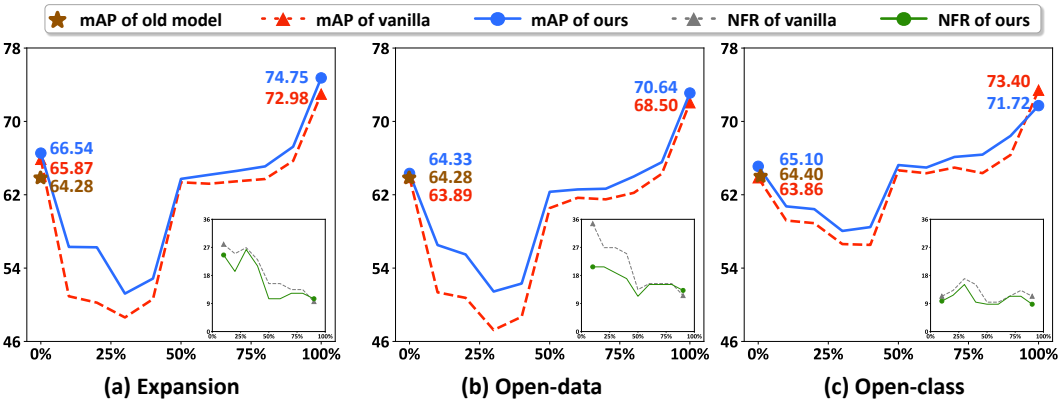

Figure 4: The trend of retrieval performance during the hot-refresh model upgrades (R50-R101) on Oxford5k, in terms of mAP(↑) and NFR(↓). Evident model regression can be observed for vanilla models, and our method alleviates this issue to a large extent.

Evaluation Metric. Mean Average Precision (**mAP**) is adopted here for evaluating the retrieval performance. Following the evaluation protocols in (Budnik & Avrithis, 2020; Weyand et al., 2020), we use mAP@100 for GLDv2-test, and mAP@10 for Oxford5k and Paris6k. Since mAP measures the overall accuracy with the consideration of both positive flips and negative flips, we define a metric, namely negative flip rate (**NFR**), to measure the degree of model regression in hot-refresh model upgrades. Note that our NFR is specifically defined for image retrieval tasks, different from the one introduced in (Yan et al., 2020). Our NFR is formulated as

$$\text{NFR@}k = \frac{|\hat{\mathcal{Q}}_k^+ \cap \mathcal{Q}_k^-|}{|\hat{\mathcal{Q}}_k^+|}, \tag{12}$$

where $\hat{\mathcal{Q}}_k^+$ denotes the set of queries that correctly recall relative images from the old gallery in top-k candidates. $\mathcal{Q}_k^-$ is the set of queries that fail to be recalled by top-k galleries during upgrading, where the gallery is a mix-up of both old and new features. NFR@1 is used in this paper.

Architectures. We study two kinds of architecture combinations, (1) **R50-R101**: ResNet-50 (He et al., 2016) for the old model, and ResNet-101 for the new model; (2) **R50-R50**: ResNet-50 for both old and new models. Due to space limitation, we discuss R50-R101 in the main paper, and the results of R50-R50 can be found in Appendix A.3. Training details can be found in Appendix A.2.

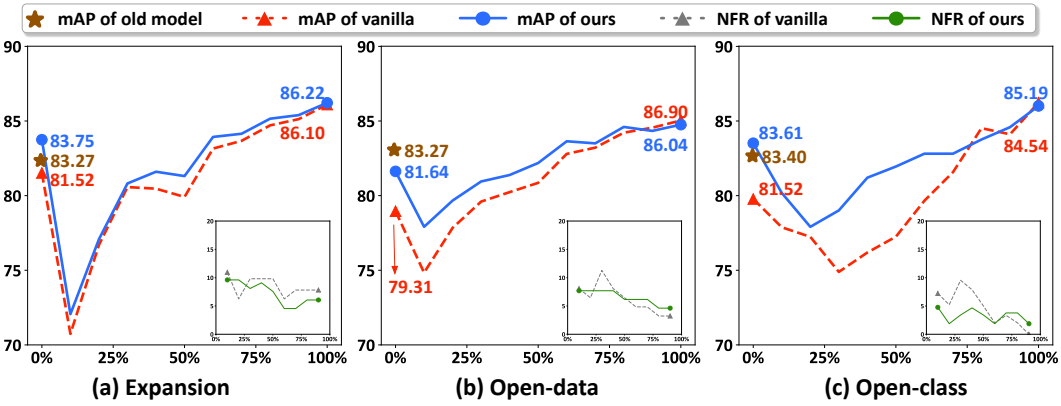

Figure 5: The trend of retrieval performance during the hot-refresh model upgrades (R50-R101) on Paris6k, in terms of mAP(↑) and NFR(↓). Our method consistently alleviates the issue of model regression on three different training data allocations. The new-to-old compatible mAP at 0% of our model is lower than the old-to-old mAP on the open-data setup, showing the same issue as the vanilla model. It is mainly due to the limited generalization ability of compatible features trained with a sole contrastive loss. Note that in this paper, we aim to study the regression-free regularization rather than advanced compatibility constraints.

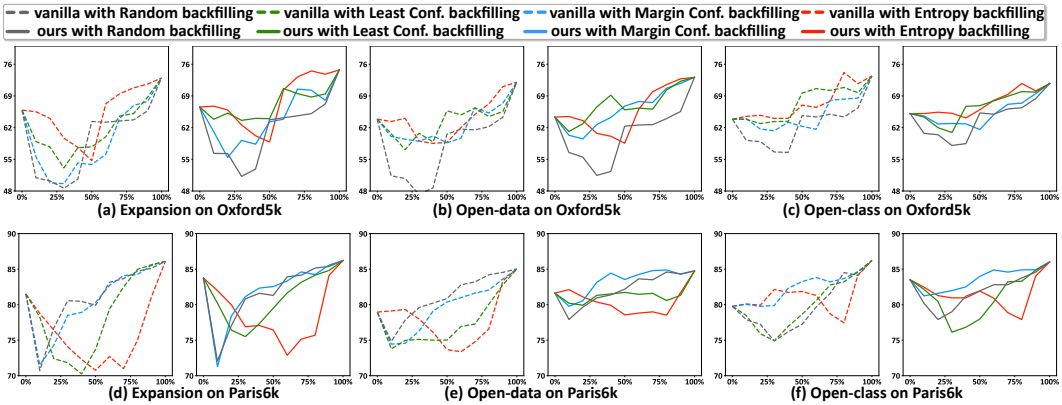

Figure 6: Comparisons between random backfilling and our introduced uncertainty-based backfilling. Results of R50-R101 are reported in terms of mAP(↑). We observe that, with either the vanilla models or our models, the uncertainty-based backfilling generally achieves faster mAP convergence. We investigate three kinds of uncertainty, and find that Least Confidence (Eq. (9)) and Margin of Confidence (Eq. (10)) generally achieve better performance than Entropy-based (Eq. (11)), indicating that the probabilities of top-2 confident classes are more important than the overall classes.

5.2 Regression-Free Compatible Training

We start with the architecture combination of R50-R101, *i.e.*, ResNet-50 for the old model, and ResNet-101 for the new one. To verify that our regression-free compatibility regularization (Eq. (6)) can properly alleviate the issue of model regression, we compare our method to the vanilla compatible training, *i.e.*, $\mathcal{L}_{\text{vanilla}}(x) = \mathcal{L}_{\text{cls}}(x) + \lambda \mathcal{L}_{\text{comp}}(x)$, where $\mathcal{L}_{\text{cls}}$ is defined in Eq. (7), and $\mathcal{L}_{\text{comp}}$ is defined in Eq. (5). Our uncertainty-based backfilling strategy is not used in this section in order to fairly compare with the vanilla settings. The only variable here is the compatibility regularization, *i.e.*, $\mathcal{L}_{\text{comp}}$ for **vanilla** and $\mathcal{L}_{\text{rf-comp}}$ for **ours**. We evaluate the models trained with expansion, open-data and open-class datasets (see Table 1) by testing on three different test sets, *i.e.*, GLDv2-test, Oxford5k, and Paris6k, as illustrated in Figure 3, 4, 5, respectively.

5.3 Uncertainty-based Backfilling

The uncertainty-based backfilling strategy is proposed to refresh the gallery following "the-poor-first" priority, in order to fasten the accuracy improvements of the image retrieval during hot-refresh

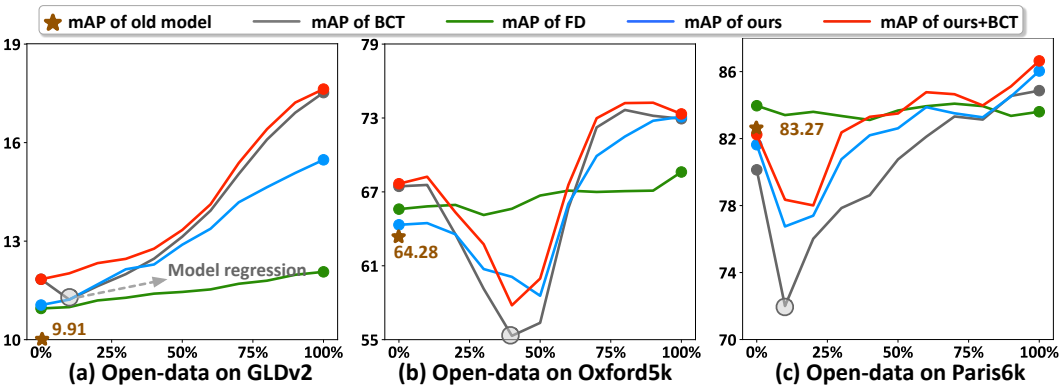

Figure 7: Comparison with two related methods, BCT (Shen et al., 2020) and Focal Distillation (FD) (Yan et al., 2020). The former one only regularizes the feature compatibility while ignoring model regression, and the latter one is specially designed for model regression of classification tasks. We achieve the optimal performance by using our regression-free compatible loss on top of BCT. Our paper studies the problem of model regression rather than advanced compatibility constraints. It is normal to use our method with more advanced compatibility losses for better performance in practice. Results of R50-R101 are reported in terms of mAP(↑).

upgrading. We discuss different backfilling strategies on Oxford5k and Paris6k, respectively, as shown in Figure 6. The uncertainty-based backfilling is plug-and-play with different models. The Least Confidence and Margin of Confidence generally achieve better performance than Entropy-based uncertainty. How to achieve faster and smoother mAP improvements during backfilling is a new task, and first investigated in this paper. Further studies are called for.

5.4 Comparison to Related Works

We discuss two important related works in this section. One is BCT (Shen et al., 2020), which only considers the feature compatibility but overlooks the model regression problem. The other is Focal Distillation (FD) (Yan et al., 2020), which discusses the model regression problem in image classification. As the definition of model regression in image classification differs from the one in image retrieval, FD is inapplicable in image retrieval tasks. As demonstrated in Figure 7, BCT suffers from the model regression, and FD achieves unsatisfactory retrieval performances. In contrast, our method could well reduce negative flips and alleviate the model regression.

6 Conclusion and Discussion

This paper for the first time studies the issue of model regression during the hot-refresh model upgrades for image retrieval systems. We hope it can arouse more public attention to the bottleneck of efficient model upgrades in industrial applications. Despite that the introduced regression-free compatibility regularization can properly reduce the negative flips to some extent, there is still a long way to go for completely wiping out the problem of model regression. Specifically, several open questions are worth investigating. (1) In this paper, we only consider the negative flips during the gallery backfilling procedure, however, there may also exist negative flips after the backfilling is finished. Maintaining the consistency of positive queries between old and new models is worth study. (2) We investigate regression-free regularization in the form of a plain contrastive loss. It may further help if integrating the regression-free regularization into more advanced backward-compatible losses. (3) Besides the backward-compatible training, forward-compatible training (Meng et al., 2021; Wang et al., 2020) may further improve the efficiency of hot-refresh model upgrades, *i.e.*, backfilling the gallery images with a forward-compatible module rather than the entire network. How to properly alleviate the negative flips with forward-compatible features remains an open question. (4) We introduce to backfill the gallery in "the-poor-first" priority with uncertainty estimation. It is also a new task for model upgrades. Future works are required for achieving faster and more stable accuracy improvements.

REPRODUCIBILITY STATEMENT

We demonstrate the core of the algorithm in the form of pseudo codes, as shown in Alg. 1 and 2. The training details and hyper-parameters can be found at Appendix A.2. The datasets are all publicly available and the training data splits are carefully illustrated in Table 1. The full code will be released upon acceptance.

Algorithm 1 Pseudocode of Regression-Free Compatible Training in a PyTorch-like style.

```
# old_model: pretrained and fixed old encoder, no gradient
# new_model: new encoder, new_model.fc is the classifier
# w: loss weight, \lambda in the paper
# tau: temperature, \tau in the paper

for (x, targets) in loader: # load a mini-batch x with N samples
   x_old = aug(x) # a randomly augmented version
   x_new = aug(x) # another randomly augmented version

   with torch.no_grad():
      old_feat = old_model.forward(x_old) # tensor shape: NxD
   new_feat = new_model.forward(x_new)

   # Classification loss, Eqn.(7)
   cls_logits = new_model.fc(new_feat)
   cls_loss = CrossEntropyLoss(cls_logits, targets)

   # select intra-class samples
   masks = targets.expand(N, N).eq(targets.expand(N, N).t())

   # positive logits: Nx1
   l_pos = bmm(new_feat.view(N,1,D), old_feat.view(N,D,1))

   # negative logits: NxN
   # exclude intra-class samples
   l_neg_n2n = mm(new_feat.view(N,D), new_feat.view(D,N)) - masks*1e9
   l_neg_n2o = mm(new_feat.view(N,D), old_feat.view(D,N)) - masks*1e9

   # logits: Nx(1+2N)
   logits = cat([l_pos, l_neg_n2n, l_neg_n2o], dim=1)

   # regression-free compatibility loss, Eqn.(6)
   labels = zeros(N) # positives are the 0-th
   rf_comp_loss = CrossEntropyLoss(logits/tau, labels)

   # SGD update: new model
   loss = cls_loss + w*rf_comp_loss
   loss.backward()
   update(new_model.params)
```

`bmm`: batch matrix multiplication; `mm`: matrix multiplication; `cat`: concatenation; `t()`: matrix transpose.

Algorithm 2 Pseudocode of Calculating Uncertainty-based Backfilling Order in a PyTorch style.

```
# N: the number of images in the gallery
# C: the number of classes in the new classifier

def cal_backfilling_order(old_feat, uncertainty_strategy='margin'):
   with torch.no_grad():
      logits = new_model.fc(old_feat) # shape: NxC
   probs = sort(softmax(logits, dim=1), dim=1)

   if uncertainty_strategy == 'least':
      # (1) Least Confidence Uncertainty, Eqn. (9)
      uncertainty_scores = 1 - probs[:,0]
   elif uncertainty_strategy == 'margin':
      # (2) Margin of Confidence Uncertainty, Eqn. (10)
      uncertainty_scores = 1 - (probs[:,0] - probs[:,1])
   elif uncertainty_strategy == 'entropy':
      # (3) Entropy-based Uncertainty, Eqn. (11)
      uncertainty_scores = - sum(probs * log(probs + 1e-9), dim=1)
   else:
      # random backfilling
      return random.shuffle(range(N))

   return argsort(uncertainty_scores) # the-poor-first priority
```

`sum`: sum all elements; `log`: logarithm; `sort`: sort the elements in descending order; `argsort`: the sorted indices in descending order.

REFERENCES

Relja Arandjelovic, Petr Gronat, Akihiko Torii, Tomas Pajdla, and Josef Sivic. Netvlad: Cnn architecture for weakly supervised place recognition. In *IEEE Conf. Comput. Vis. Pattern Recog.*, pp. 5297–5307, 2016.

Slawomir Bak and Peter Carr. One-shot metric learning for person re-identification. In *IEEE Conf. Comput. Vis. Pattern Recog.*, pp. 2990–2999, 2017.

Andrew Brown, Weidi Xie, Vicky Kalogeiton, and Andrew Zisserman. Smooth-ap: Smoothing the path towards large-scale image retrieval. In *Eur. Conf. Comput. Vis.*, pp. 677–694. Springer, 2020.

Mateusz Budnik and Yannis Avrithis. Asymmetric metric learning for knowledge transfer. *arXiv preprint arXiv:2006.16331*, 2020.

Xiangyong Cao, Jing Yao, Zongben Xu, and Deyu Meng. Hyperspectral image classification with convolutional neural network and active learning. *IEEE Transactions on Geoscience and Remote Sensing*, 2020.

Yuntao Chen, Naiyan Wang, and Zhaoxiang Zhang. Darkrank: Accelerating deep metric learning via cross sample similarities transfer. In *AAAI*, 2018.

Zhen Cui, Wen Li, Dong Xu, Shiguang Shan, and Xilin Chen. Fusing robust face region descriptors via multiple metric learning for face recognition in the wild. In *IEEE Conf. Comput. Vis. Pattern Recog.*, pp. 3554–3561, 2013.

Jia Deng, Wei Dong, Richard Socher, Li-Jia Li, Kai Li, and Li Fei-Fei. Imagenet: A large-scale hierarchical image database. In *IEEE Conf. Comput. Vis. Pattern Recog.* Ieee, 2009.

Rahul Duggal, Hao Zhou, Shuo Yang, Yuanjun Xiong, Wei Xia, Zhuowen Tu, and Stefano Soatto. Compatibility-aware heterogeneous visual search. *arXiv preprint arXiv:2105.06047*, 2021.

Yixiao Ge, Dapeng Chen, and Hongsheng Li. Mutual mean-teaching: Pseudo label refinery for unsupervised domain adaptation on person re-identification. In *Int. Conf. Learn. Represent.*, 2020a.

Yixiao Ge, Haibo Wang, Feng Zhu, Rui Zhao, and Hongsheng Li. Self-supervising fine-grained region similarities for large-scale image localization. In *Eur. Conf. Comput. Vis.*, 2020b.

Yixiao Ge, Feng Zhu, Dapeng Chen, Rui Zhao, and Hongsheng Li. Self-paced contrastive learning with hybrid memory for domain adaptive object re-id. In *Adv. Neural Inform. Process. Syst.*, 2020c.

Albert Gordo, Jon Almazán, Jerome Revaud, and Diane Larlus. Deep image retrieval: Learning global representations for image search. In *Eur. Conf. Comput. Vis.* Springer, 2016.

Matthieu Guillaumin, Jakob Verbeek, and Cordelia Schmid. Is that you? metric learning approaches for face identification. In *Int. Conf. Comput. Vis.*, pp. 498–505. IEEE, 2009.

Kaiming He, Xiangyu Zhang, Shaoqing Ren, and Jian Sun. Deep residual learning for image recognition. In *IEEE Conf. Comput. Vis. Pattern Recog.*, 2016.

Geoffrey Hinton, Oriol Vinyals, and Jeff Dean. Distilling the knowledge in a neural network. *arXiv preprint arXiv:1503.02531*, 2015.

Alex Holub, Pietro Perona, and Michael C Burl. Entropy-based active learning for object recognition. In *IEEE Conf. Comput. Vis. Pattern Recog. Worksh.*, 2008.

SeungKee Jeon. 1st place solution to google landmark retrieval 2020. *arXiv preprint arXiv:2009.05132*, 2020.

Changlin Li, Jiefeng Peng, Liuchun Yuan, Guangrun Wang, Xiaodan Liang, Liang Lin, and Xiaojun Chang. Block-wisely supervised neural architecture search with knowledge distillation. In *IEEE Conf. Comput. Vis. Pattern Recog.*, pp. 1989–1998, 2020a.

Shaohua Li, Xiuchao Sui, Jie Fu, Yong Liu, and Rick Siow Mong Goh. Feature lenses: Plug-and-play neural modules for transformation-invariant visual representations. *arXiv preprint arXiv:2004.05554*, 2020b.

Wei Li, Rui Zhao, Tong Xiao, and Xiaogang Wang. Deepreid: Deep filter pairing neural network for person re-identification. In *IEEE Conf. Comput. Vis. Pattern Recog.*, 2014.

Zhizhong Li and Derek Hoiem. Learning without forgetting. *IEEE Trans. Pattern Anal. Mach. Intell.*, 40(12):2935–2947, 2018. doi: 10.1109/TPAMI.2017.2773081.

Zimo Liu, Dong Wang, and Huchuan Lu. Stepwise metric promotion for unsupervised video person re-identification. In *Int. Conf. Comput. Vis.*, pp. 2429–2438, 2017.

Qiang Meng, Chixiang Zhang, Xiaoqiang Xu, and Feng Zhou. Learning compatible embeddings. In *Int. Conf. Comput. Vis.*, 2021.

James Philbin, Ondrej Chum, Michael Isard, Josef Sivic, and Andrew Zisserman. Object retrieval with large vocabularies and fast spatial matching. In *IEEE Conf. Comput. Vis. Pattern Recog.*, pp. 1–8. IEEE, 2007.

James Philbin, Ondrej Chum, Michael Isard, Josef Sivic, and Andrew Zisserman. Lost in quantization: Improving particular object retrieval in large scale image databases. In *IEEE Conf. Comput. Vis. Pattern Recog.*, pp. 1–8. IEEE, 2008.

Filip Radenović, Ahmet Iscen, Giorgos Tolias, Yannis Avrithis, and Ondřej Chum. Revisiting oxford and paris: Large-scale image retrieval benchmarking. In *IEEE Conf. Comput. Vis. Pattern Recog.*, 2018.

Burr Settles. Active learning literature survey. 2009.

Yantao Shen, Yuanjun Xiong, Wei Xia, and Stefano Soatto. Towards backward-compatible representation learning. In *IEEE Conf. Comput. Vis. Pattern Recog.*, 2020.

Megha Srivastava, Besmira Nushi, Ece Kamar, Shital Shah, and Eric Horvitz. An empirical analysis of backward compatibility in machine learning systems. In *Proceedings of the 26th ACM SIGKDD International Conference on Knowledge Discovery & Data Mining*, 2020.

Yi Sun, Yuheng Chen, Xiaogang Wang, and Xiaoou Tang. Deep learning face representation by joint identification-verification. In *Advances in neural information processing systems*, 2014a.

Yi Sun, Xiaogang Wang, and Xiaoou Tang. Deep learning face representation from predicting 10,000 classes. In *IEEE Conf. Comput. Vis. Pattern Recog.*, 2014b.

Chien-Yi Wang, Ya-Liang Chang, Shang-Ta Yang, Dong Chen, and Shang-Hong Lai. Unified representation learning for cross model compatibility. *Brit. Mach. Vis. Conf.*, 2020.

Tobias Weyand, Andre Araujo, Bingyi Cao, and Jack Sim. Google landmarks dataset v2-a large-scale benchmark for instance-level recognition and retrieval. In *IEEE Conf. Comput. Vis. Pattern Recog.*, 2020.

Yuqing Xie, Yi-an Lai, Yuanjun Xiong, Yi Zhang, and Stefano Soatto. Regression bugs are in your model! measuring, reducing and analyzing regressions in nlp model updates. *arXiv preprint arXiv:2105.03048*, 2021.

Sijie Yan, Yuanjun Xiong, Kaustav Kundu, Shuo Yang, Siqi Deng, Meng Wang, Wei Xia, and Stefano Soatto. Positive-congruent training: Towards regression-free model updates. *arXiv preprint arXiv:2011.09161*, 2020.

Liang Zheng, Liyue Shen, Lu Tian, Shengjin Wang, Jingdong Wang, and Qi Tian. Scalable person re-identification: A benchmark. In *Int. Conf. Comput. Vis.*, 2015.

Kaiyang Zhou, Yongxin Yang, Andrea Cavallaro, and Tao Xiang. Omni-scale feature learning for person re-identification. In *Int. Conf. Comput. Vis.*, pp. 3702–3712, 2019.

Jingbo Zhu, Huizhen Wang, Tianshun Yao, and Benjamin K Tsou. Active learning with sampling by uncertainty and density for word sense disambiguation and text classification. In *Proceedings of the 22nd International Conference on Computational Linguistics (Coling 2008)*, 2008.

A APPENDIX

A.1 ADDITIONAL RELATED WORKS

Knowledge Distillation. Knowledge distillation (Hinton et al., 2015; Li et al., 2020a) aims at training a student (new) model that inherits the "dark knowledge" of the teacher (old) model. Although knowledge distillation and our task both regularize the prediction consistency between two different models, we have entirely different targets, *i.e.*, knowledge distillation aims at improving the overall accuracy of the new model while our task requires to reduce negative flips during cross-model retrieval. The techniques of knowledge distillation cannot solve the model regression problem in hot-refresh model upgrades of retrieval tasks.

A.2 TRAINING DETAILS

The networks are pre-trained on the ImageNet dataset (Deng et al., 2009). The images are resized to 224×224 for both training and testing. During training, random data augmentation is applied to each image before it is fed into the network, including randomly flipping and cropping. We adopt 6 Tesla V100 GPUs for training, and the batch size per GPU is set to 80 for ResNet-50 and 64 for ResNet-101. For all the experiments, Adam optimizer is adopted to optimize the training model with a weight decay of 0.0001. The initial learning rate is set to 0.01 and is decreased to 1/10 of its previous value every 30 epochs in the total 90 epochs. The old model is trained with only a classification loss in Eq. (7), and the new model is trained towards the objective in Eq. (8). The temperature τ in Eq. (6) is empirically set as 0.05, and the loss weight λ in Eq. (8) is set as 1.0.

A.3 MODEL UPGRADES OF THE SAME ARCHITECTURE

Regression-Free Compatible Training. We further evaluate our method when the new model has the same architecture as the old model, *e.g.*, ResNet-50 for both old and new models. As illustrated in Figure 8, the retrieval system with vanilla models is less susceptible to the model regression problem compared to the R50-R101 setup (Figure 3) when testing on GLDv2-test. This is because that old and new models of the same architecture start from the same weights, *i.e.*, ImageNet pre-training. They have natural prediction consistency in the beginning, making the feature compatibility easier. Even so, we argue that vanilla models show evident larger NFR than our model, indicating an underlying model regression. The results of Oxford5k and Paris6k can be found in Figure 9, 10.

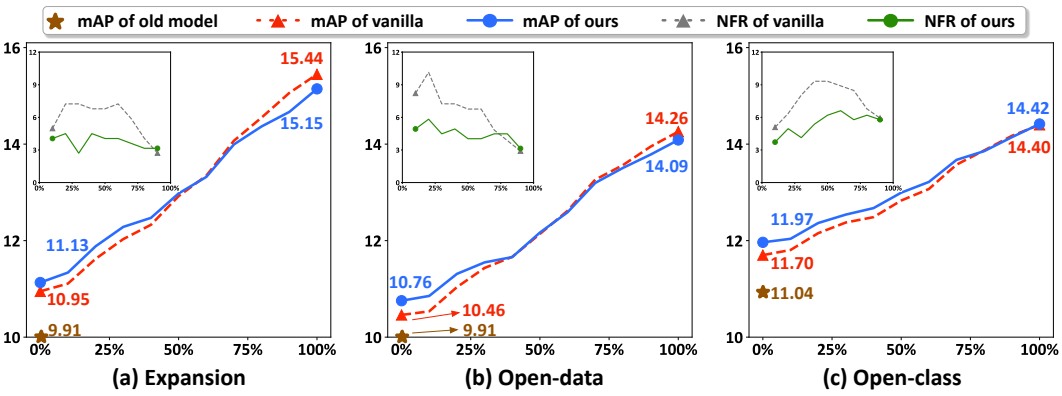

Figure 8: The trend of retrieval performance during the hot-refresh model upgrades of the same architecture, *i.e.*, R50-R50. The results are reported on GLDv2-test in terms of mAP(↑) and NFR(↓). We observe that, despite the overall accuracy (*i.e.*, mAP) has gradually increased without regression, vanilla shows significantly larger NFR than ours. Noted that even if the overall mAP has increased, every new mistake on the old positive queries feels like a step backwards, still leading to a perceived regression in user experience. Reducing NFR can be as important as improving mAP in practice.

Uncertainty-based Backfilling. We investigate the uncertainty-based backfilling on the setup of R50-R50, as shown in Figure 11. Backfilling the gallery with uncertainty-based priority can effectively fasten the performance improvements of image retrieval systems.

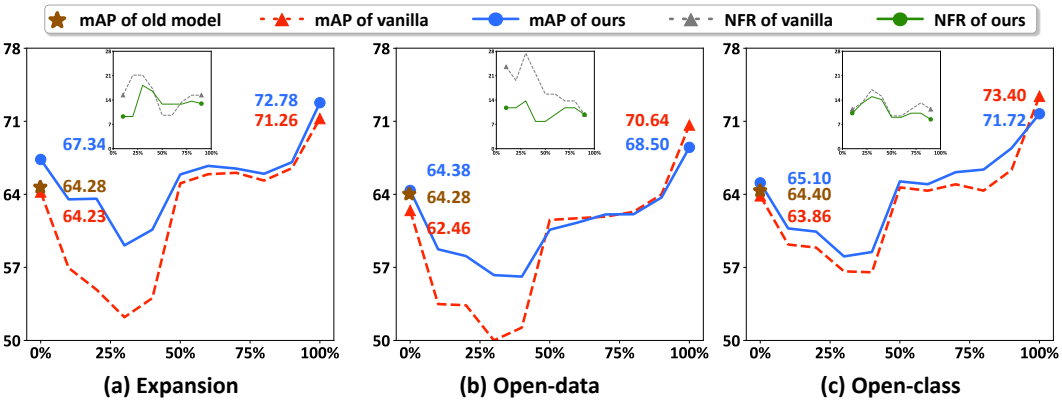

Figure 9: The trend of retrieval performance during the hot-refresh model upgrades (R50-R50) on Oxford5k, in terms of mAP(↑) and NFR(↓).

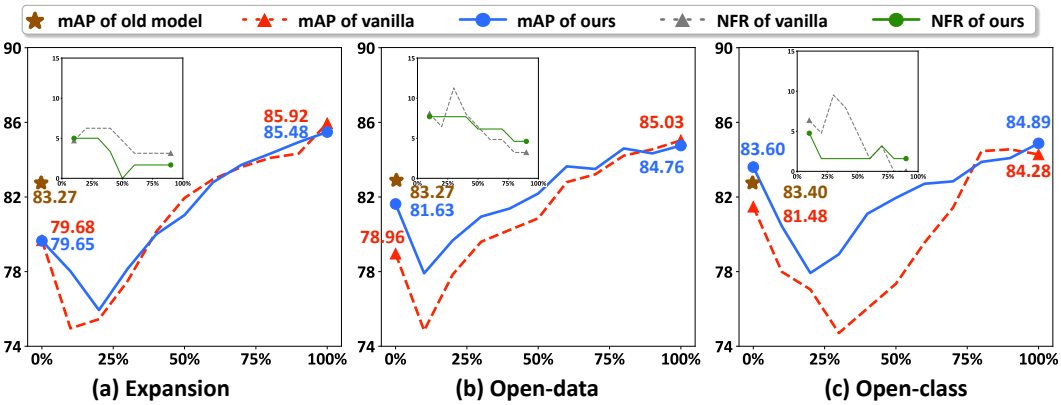

Figure 10: The trend of retrieval performance during the hot-refresh model upgrades (R50-R50) on Paris6k, in terms of mAP(↑) and NFR(↓). Our method consistently alleviates the issue of model regression on three different training data allocations. The new-to-old compatible mAP at 0% of our model is lower than the old-to-old mAP on expansion and open-data setups, showing the same issue as the vanilla model. It is mainly due to the limited generalization ability of compatible features trained with a sole contrastive loss.

Compare to BCT (Shen et al., 2020) and FD (Yan et al., 2020). We have discussed two critical related works in the main paper, *i.e.*, BCT (Shen et al., 2020) and FD (Yan et al., 2020). BCT, for the first time, introduces backward-compatible training in computer vision. However, as it only focuses on the backfill-free model upgrades, it overlooks the hot-refresh model upgrades and the problem of model regression. FD investigates the problem of model regression in image classification tasks. The constraints are not specially designed to adapt the image retrieval tasks, leading to unsatisfactory performances. The results on the setup of R50-R50 can be found in Figure 12.

A.4 Ablation Studies

Effects of temperature τ. The temperature τ is empirically set as 0.05 in this work. We discuss different values of τ in Table 2. A similar increasing trend of retrieval performance upgrades can be observed when τ varies from 0.05 to 0.1, while model regression at 20% is observed when $\tau = 0.01$. The 100% new-to-new performances are sub-optimal when $\tau = 0.1$ and $\tau = 0.08$. In all, 0.05 is a suitable value for the contrastive temperature, and all the experiments in this paper adopt the same temperature value for a fair comparison.

Effects of loss weight λ. The loss weight λ is set as 1.0 in this work for simplicity. We study the effects of different λ in Table 3. We can observe that the value of λ controls the trade-off between new feature discriminativeness and new-to-old feature compatibility, *i.e.*, models with smaller λ achieve

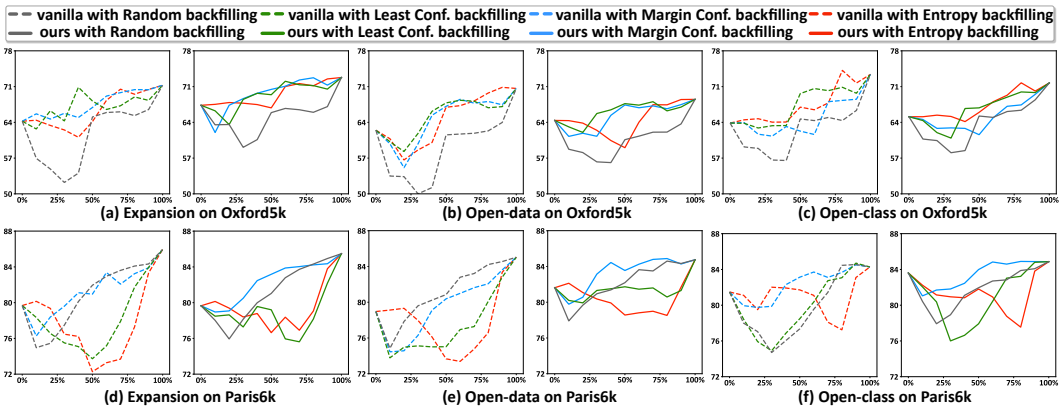

Figure 11: Comparisons between random backfilling and our introduced uncertainty-based backfilling, in terms of mAP(↑). Results of R50-R50 are reported. We find that Margin of Confidence (Eq. (10)) is relatively optimal.

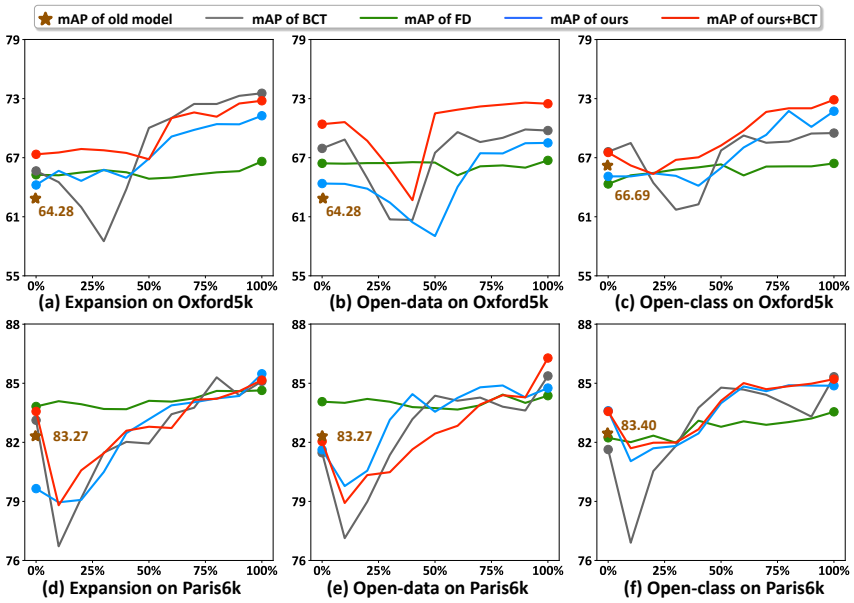

Figure 12: Compare to BCT (Shen et al., 2020) and FD (Yan et al., 2020) on Oxford5k and Paris6k. Results of R50-R50 are reported in terms of mAP(↑).

better performance at 100% while models with larger λ achieve better performance at 0%. Despite the start and end points vary from different models, a similar increasing trend of the performances during backfilling can be observed.

Effects of batch size. We use a batch size of 80 per GPU for the experiments with ResNet-50. As the batch size may affect the number of negative samples for contrastive loss, we conduct ablation studies by modifying the batch size, as illustrated in Table 4. We observe that our method is robust to the number of batch size.

Effects of positive sampler. As mentioned in the method, for more efficient training, we treat the compatible training as an instance discrimination task when training with the large-scale retrieval dataset, *i.e.*, GLDv2. Specifically, the positive pair consists of the new and old features of the same instance, since it is hard to make sure intra-class instances exist in the same mini-batch without a pre-sampler. To verify that the mentioned instance discrimination-like compatible training does not harm the retrieval performance, we conduct an ablation study by using a positive pre-sampler to randomly sample an intra-class sample for each anchor before each iteration. As shown in Table 5, similar results can be achieved by using either the positive pre-sampler or not.

τ	old	0%	20%	40%	60%	80%	100%
0.1	9.91	11.13(+1.22)	11.44(+0.30)	11.70(+0.26)	12.05(+0.35)	12.57(+0.52)	13.28(+0.71)
0.08	9.91	11.24(+1.33)	11.65(+0.40)	11.96(+0.31)	12.29(+0.33)	12.97(+0.68)	13.73(+0.76)
0.05	9.91	11.13(+1.22)	11.88(+0.75)	12.47(+0.59)	13.32(+0.85)	14.37(+1.05)	15.14(+0.78)
0.01	9.91	10.34(+0.43)	10.07(-0.27)	10.54(+0.46)	12.55(+2.01)	15.12(+2.57)	15.87(+0.74)

Table 2: Performance of our method with different values of temperature τ in terms of mAP(↑). The results are reported on GLDv2-test with the architectures of R50-R50.

λ	old	0%	20%	40%	60%	80%	100%
0.1	9.91	10.66(+0.75)	10.66(+0.00)	11.28(+0.62)	12.66(+1.38)	14.34(+1.67)	15.64(+1.31)
0.5	9.91	10.94(+1.03)	11.71(+0.77)	12.24(+0.53)	13.19(+0.95)	14.31(+1.12)	15.07(+0.76)
1	9.91	11.13(+1.22)	11.88(+0.75)	12.47(+0.59)	13.32(+0.85)	14.37(+1.05)	15.14(+0.78)
2	9.91	11.10(+1.19)	11.77(+0.67)	12.37(+0.60)	13.16(+0.79)	13.97(+0.81)	14.76(+0.79)
5	9.91	11.24(+1.33)	11.79(+0.55)	12.17(+0.38)	12.60(+0.43)	13.34(+0.75)	14.32(+0.97)

Table 3: Performance of our method with different values of loss weight λ in terms of mAP(↑). The results are reported on GLDv2-test with the architectures of R50-R50.

b.s.	old	0%	20%	40%	60%	80%	100%
40	9.91	10.98(+1.07)	11.83(+0.85)	12.51(+0.68)	13.53(+1.01)	14.79(+1.26)	15.77(+0.99)
60	9.91	11.05(+1.14)	11.81(+0.76)	12.53(+0.71)	13.43(+0.91)	14.50(+1.06)	15.34(+0.85)
80	9.91	11.13(+1.22)	11.88(+0.75)	12.47(+0.59)	13.32(+0.85)	14.37(+1.05)	15.14(+0.78)

Table 4: Performance of our method with different batch size (b.s.) per GPU in terms of mAP(↑). The results are reported on GLDv2-test with the architectures of R50-R50. We fail to try larger batch sizes due to the GPU memory limitation.

Sampler	old	0%	20%	40%	60%	80%	100%
w/	9.91	11.41(+1.50)	12.11(+0.70)	12.65(+0.53)	13.41(+0.76)	14.33(+0.92)	15.08(+0.76)
w/o	9.91	11.13(+1.22)	11.88(+0.75)	12.47(+0.59)	13.32(+0.85)	14.37(+1.05)	15.14(+0.78)

Table 5: Compare to the results when adopting a positive pre-sampler. The results are reported on GLDv2-test with the architectures of R50-R50, in terms of mAP(↑). Using the positive pre-sampler achieves slightly better performance at 0%, but lower training efficiency. Similar final performances can be achieved with either the sampler or not, so we discard the positive sampler for more efficient training with large-scale datasets.